Astron. Astrophys. 323, 749–761 (1997)

ASTRONOMY
AND
ASTROPHYSICS

Kinematics and stellar populations in active galaxies: the LINER NGC 4579 (M58)

J. Palacios[1], **M.L. García-Vargas**[2], **Angeles Díaz**[1], **Roberto Terlevich**[3], **and Elena Terlevich**[4]

[1] Dpto. de Física Teórica, Facultad de Ciencias, C-XI. Cantoblanco. Universidad Autónoma de Madrid, E-28049 Madrid, Spain
[2] INSA; ESA IUE Observatory, Villafranca del Castillo Satellite Tracking Station, PO Box 50727, E-28080 Madrid, Spain
[3] Royal Greenwich Observatory, Madingley Road, Cambridge CB30EZ, UK
[4] Institute of Astronomy, Madingley Road, Cambridge CB30HA, UK

Received 10 May 1996 / Accepted 13 January 1997

Abstract. We present long slit spectroscopy from the blue to the near-IR of the LINER galaxy NGC 4579 (M58). Stellar indices are used as tools to investigate if any differences in the kinematics and/or stellar content exist between the nucleus and the circumnuclear regions of the galaxy. Blue indices are found to be affected by contamination due to emission lines in the central region and the method to measure these indices is discussed. No peculiarities are found in the stellar kinematics with respect to the bulges of normal spirals, whose old population can fit the observations of the bulge of NGC 4579. Alternatively, the low central values of Mg_2 and the high values of Mg_1 in the blue and MgI in the near-IR lead us to propose the dominant bulge stellar population in NGC 4579 to be substantially younger than the one present in ordinary ellipticals and S0 galaxies, and therefore a population with an age of about (2.5 ± 1) Gyr. and a metallicity of (1.5 ± 0.5) $Z_\odot$ is also able to reproduce simultaneously the studied spectral indices as well as the optical spectral energy distribution of the nucleus of NGC 4579.

Key words: galaxies: NGC 4579(M58) – active – kinematics and dynamics – stellar content

1. Introduction

Although the interest in the properties of galaxies which host active galactic nuclei (AGN) has increased in the last years, still there are few studies which refer to the stellar populations and kinematical properties of these objects. Contamination by the emission line spectrum arising from the ionized gas and lack of spatial resolution constitute the main technical difficulties involved in the project.

Prominent stellar lines in the optical and near-IR spectral regions can be used to characterize the stellar populations dominating the light at those wavelengths as well as to study their corresponding rotation and velocity dispersions. If long slit observations are used the spatial behaviour of these properties can be explored.

This is the first one of two papers in which the magnesium spectral indices (atomic Mgb, molecular Mg_1 and Mg_2) and Fe_{52} in the blue and the Ca II triplet, CaT, and MgI in the near-IR are used to study the kinematics and stellar populations in the central 10 arcsec of nearby active galaxies. Since LINERs are the least active of AGN, they are probably the best candidates to undertake such a study since the continuum is dominated by stellar light in the optical and near infrared. This is the reason to devote this first paper to discuss in detail the results for the LINER NGC 4579 (M58). In a following paper, we will analyze the results for three Seyfert galaxies: NGC 5953, NGC 6814 and NGC 7469.

The galaxy NGC 4579, M58, is located at about 20 Mpc (cz = 1502 Km/s, Véron-Cetty & Véron 1993) and is a member of the Virgo cluster. It has a morphological type SBb (de Vaucoleurs et al. 1991), and was classified as LINER by Filippenko & Sargent (1985) who reported the evidence of weak broad H_α emission, already detected by Stauffer (1982). Keel (1983) published an H_α + [NII] narrow band image noting a *weak spiral pattern* northeast of the nucleus. This feature was observed later as a loop of emission by Pogge (1989) and interpreted as the reminiscent of the emission bubbles associated with radio-structures in low luminosity AGN. The extended emission observed in H_α + [NII] amounts to 62% of the total. Long slit spectroscopy along the loop and in the circumnuclear region is reported by González-Delgado & Pérez (1996). According to them, [OIII] imaging shows a stellar-source nuclear appearance, implying a relatively low ionization state. A nuclear flat spectrum radio core was reported by Hummel et al. (1984; 1987, 1990), as well as X-ray emission (Halpern & Steiner 1983).

IUE data by Kinney et al. (1993) show an UV continuum similar to that observed in normal galaxies, and emission lines similar to those observed in Seyfert 2 galaxies although with enhanced low ionization lines (Reichert et al. 1993). Recently, Barth et al. (1996) have presented a FOS/HST UV spectrum of

Send offprint requests to: M.L. García-Vargas

Table 1. Spectral configurations

	Spectral range (Å)	Disp (Å / pixel)	FWHM (Å)	Exp time (s)
Blue	4330 - 5618	2.28	4.0	1200
Red	5850 - 7109	2.29	3.3	600
Near-IR	7840 - 9139	2.30	3.7	1200

NGC4579. Maoz et al. (1995) report the detection in the nucleus of NGC 4579 of a bright unresolved source (< 0.11") in an UV (2300 Å) FOC image by HST. They also report a slightly extended source (PA=72^o) with flux about 15% of the brighter nuclear source and located at 0.58" from it. This detection is coincident with the detection of the optical loop. The authors suggest a star cluster as the possible ionizing source.

This paper is divided as follows: Sect. 2 summarizes the observations and data-reduction procedures. The measurement methods are described in Sect. 3, spectral indices in 3.1 and kinematics in 3.2. Sect. 4 presents the results. In particular, subsection 4.1 contains those referring to the nuclear gas kinematics, 4.2 the stellar kinematics, like the rotation curve and the velocity dispersion curve, and 4.3 the spatial gradients of the blue and near-IR spectral indices. Sect. 5 discusses the results on the basis of evolutionary synthesis models. Finally, Sect. 6 summarizes the conclusions.

2. Observations and data reduction

The observations were carried out on 1989 July 10 and 11, at the Observatorio del Roque de los Muchachos on the Spanish island of La Palma, at the Cassegrain focus of the INT 2.5 m telescope. We used the Intermediate Dispersion Spectrograph (IDS), the 235 mm camera and a CCD detector with a GEC chip. The pixel size for this setup configuration was 0.7". The slit width was 210 μm, equivalent to 1.4". Two different gratings were used to cover the wavelength range: R400V for the blue (λ_c = 4976 Å) and around H_α (λ_c = 6469 Å) and R400R for the near-IR (λ_c = 8488 Å). Two colour filters: WG360 and GC495 were used to avoid second order contamination in the H_α and IR spectra respectively. Three different wavelength ranges were chosen for observation: (a) the blue spectrum, including the Mgb, Fe_{52}, Mg_1, Mg_2 stellar features, as well as nebular emission lines: H_γ , H_β , [OIII]4363, 4959, 5007 Å, [FeII]5284, 5317, 5363 Å, (b) the red range centered at H_α for observations of the red emission line spectrum (H_α , [OI]6300, 6363; [NII]6548, 6584, [SII]6717, 6731 Å), and (c) the near-IR spectrum to observe CaT, 8498, 8542, 8662 Å and MgI 8807 Å stellar features, and the [SIII]9069 Å emission line.

The spectral ranges, grating resolutions and exposure times are given in Table 1. The object was observed with the slit at P.A. 298^o.

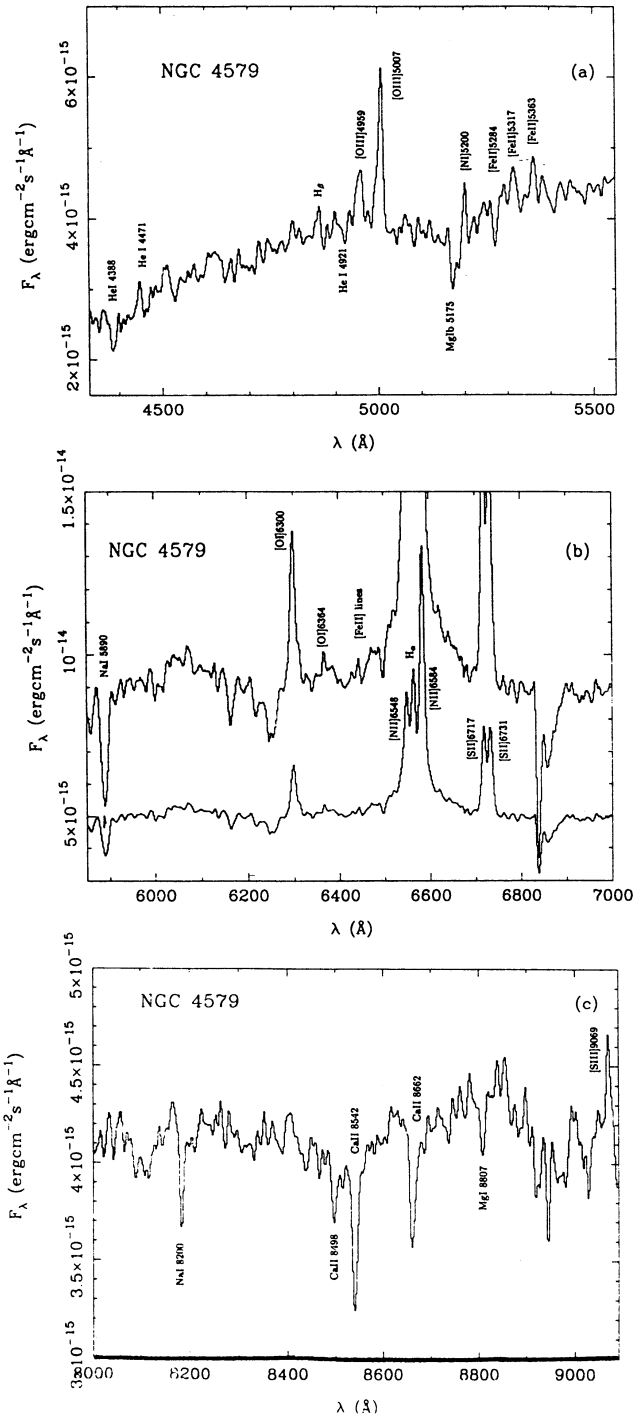

Fig. 1. Nuclear spectrum of the galaxy NGC 4579 in the blue (top), red (middle) and near-IR (bottom). The vertical scale corresponds to the spectrum in which the strongest lines are fully plotted.

Several bias, preflash images and flat-field frames in the three wavelength ranges were taken at the beginning and the end of the night. One calibration lamp exposure per spectral region and telescope position was performed. The calibration lamps used were CuAr in blue-red spectroscopy and CuAr + CuNe for near-IR spectroscopy. Two standard stars, HD140283

Table 2. Stellar reference frame

Star	Spectral type	Blue	near-IR
BD+17 4708	F6 sd	X	X
BD+26 2606	F5	X	X
HD140283	F3 sd	X	X
HR7407	K0 III	X	X
HR7813	K0 III	X	X
HR7914	G5 V	X	–
HR7942	G9 III	X	–
HR8532	F7 V	X	X
HR8784	F8 IV	X	X

and BD+17 4708, were observed in the three wavelength ranges for flux calibration.

Observations of 9 template stars in the blue and 7 in the near-IR ranges were made. These stars were selected to provide a good stellar reference frame in the same system as the galaxies for the analysis of the velocity dispersions. Table 2 lists the stars as well as their spectral types. The seeing during the observations was 1.5".

The data reduction was carried out at the Universidad Autónoma de Madrid, using *Starlink FIGARO* and *ESO MIDAS* standard software packages. The procedure includes the removal of cosmic rays, the subtraction of a dark current, bias, and the subtraction of a dark-corrected pre-flash frame, necessary due to the non-linearity of the detector for low-count level. The non-linearity is only noticeable at the CCD edges, but has to be taken into account since the CCD borders sometimes must be used for sky subtraction, a critical phase in the analysis.

After these preliminar corrections, the bi-dimensional images were divided by a normalized flat-field. Several flat-field frames were taken along the night. Their spatial profiles were controlled, comparing them with the ones from calibration arcs (one arc per observation), allowing a careful flat-field correction, specially in the CCD edges, whose importance has already been remarked.

The spectra were corrected for atmospheric extinction using a mean extinction curve appropriate for La Palma Observatory (King 1985). The assigned air-mass was the averaged value over the exposure time. Flux calibration was then achieved using two standard stars, taking the calibrated data from Oke & Gunn (1983). The errors in flux calibration are lower than 5%.

Fig. 1 shows the nuclear spectrum of NGC 4579 at the three observed wavelength ranges.

3. Measurement methods

In this work we present spatial gradients of stellar features indices and kinematical parameters (rotation and velocity dispersion curves). From the bi-dimensional frames we have extracted spectra at different values of the galactocentric distance. The number of pixels was chosen with the criterion of having enough signal to noise to measure the Mgb line in the blue and the CaT in the near IR spectra. The minimum number of pixels was 3 (according to the seeing). We oversampled the bi-dimensional profiles to improve the spatial resolution. The assigned effective radius (galactocentric distance) for each extraction was found by weighting the radius of each scan with the luminosity profile, using a emission-free continuum window. The spatial profiles with the extractions are shown in Fig. 2.

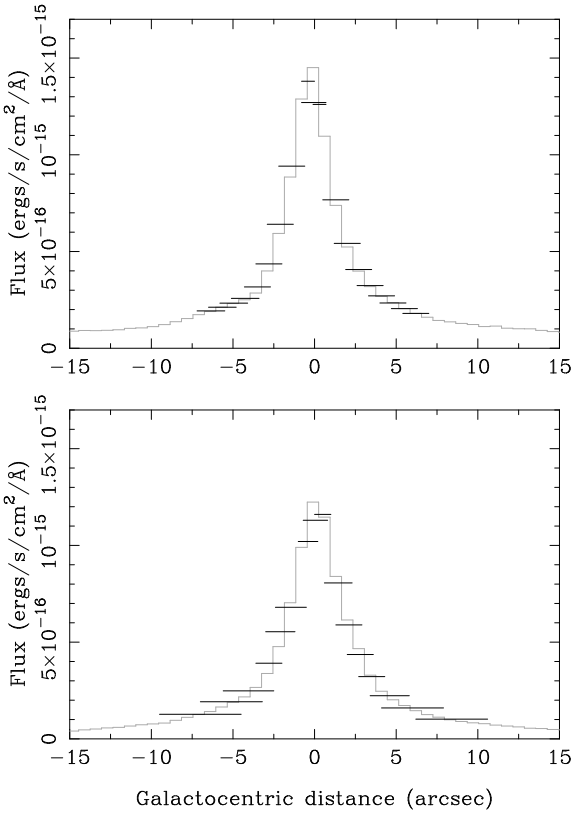

Fig. 2. Spatial profiles of the blue (top) and near-IR (bottom) two-dimensional spectra. The horizontal lines mark the extractions for the 1D individual spectra used to perform the gradients.

3.1. Spectral indices

The indices we have measured correspond to different stellar features: various magnesium indices (Mgb, Mg_1, Mg_2) and Fe_{52} in the blue range, and CaT and MgI, in the near-IR. The value of a given index depends strongly on the system in which the measurements are made, being necessary to specify a spectral window to measure the stellar feature and at least two continuum bandpasses. The pseudo-continuum used to measure the index is then defined by a linear fit to the averaged fluxes in each chosen side-spectral windows.

The definitions for the measured indices are given in Gorgas et al. (1993) for the blue features and Díaz et al. (1989) for the near-IR ones (CaT and MgI). Accordingly, the CaT index has been taken as the sum of the two strongest lines ($\lambda\lambda$ 8542, 8662 Å) pseudo equivalent widths. The windows for the features and

Table 3. Spectral features and continuum windows

Feature	Central band-pass (Å)	Continuum band-pass (Å)
		5144.50 - 5162.00
Mgb	5162.00 - 5193.25	
		5193.25 - 5207.00
		4897.00 - 4958.25
Mg_1	5071.00 - 5134.75	
		5303.00 - 5366.75
		4897.00 - 4958.25
Mg_2	5156.00 - 5197.25	
		5303.00 - 5366.75
		5235.50 - 5249.25
Fe_{52}	5248.00 - 5286.75	
		5288.00 - 5319.25
	8527.00 - 8557.00	8447.50 - 8462.50
CaT	+	
	8647.00 - 8677.00	8842.50 - 8857.50
		8775.00 - 8787.00
MgI	8799.50 - 8814.50	
		8845.00 - 8855.00

Table 4. Measured and decontaminated values of Mgb index

Radius (arcsec)	Mgb^0 Å	Mgb^1 Å	Mgb^2 Å	Mgb Å	Error Å
–0.1	5.42	3.37	3.09	3.23	0.18
+0.2	5.52	3.44	3.04	3.24	0.26
–0.4	5.55	3.55	3.04	3.29	0.26
+1.2	4.07	2.86	3.12	2.99	0.30
–1.3	4.35	2.93	3.06	3.00	0.20
+1.9	3.28	2.93	3.53	3.23	0.38
–2.0	3.52	2.16	2.86	2.51	0.35

the continuum band-passes for each index are summarized in Table 3.

Some emission lines, often present in AGN spectra can contaminate the continuum band-passes. Such is the case for [OI] λ 8440 Å at the blue side of the CaT and the emission-line doublet [NI]$\lambda\lambda$ 5197.9, 5200.4 Å(we will refer to is as [NI]λ 5200 Å) at the red side of the Mgb line, and in the central window of Mg_2 index. Therefore, in the cases in which the presence of gas is known, optional windows, or alternatively a different method to decontaminate the value of the index have to be used.

For the CaT case, Terlevich et al. (1990) proposed an optional window for the blue continuum, centered at 8582 Å and 15 Å wide. However, in the case of NGC 4579, no emission at [OI] 8440 Å is detected (see Fig. 1, bottom), and therefore the originally defined windows for CaT have been used.

In this case, [NI]5200 Å emission is seen, confined to the nucleus of the galaxy. In the following, we discuss the method used to measure the blue indices in the spectra affected by [NI] contamination (from -1.3" to +1.2"). Out of these regions, we have used the standard method and windows.

The Mgb is the index more clearly affected by [NI]λ 5200 Å contamination. Goudfrooij & Emsellem (1996, hereafter GE96) have discussed how the emission [NI]λ 5200 Å affects the Mgb line strength measurements in elliptical galaxies and spiral bulges which in some cases, after the subtraction of an old stellar population template, show emission features from ionized gas. These authors conclude that the compiled values of the Mgb index could be overestimated by up to 2 Å due to this effect.

According to GE96, it is possible to calculate the equivalent width of the [NI]5200 Å line width which is contaminating the original red continuum band-pass of the Mgb index. Therefore, we have fitted a gaussian profile to the [NI]5200 Å line, and we have integrated this profile between the wavelengths of the red window (5193.25 - 5207.00). Using formula (5) of GE96, we have calculated the EW which has to be substracted from the values of the Mgb index measured with the original band-passes, and we have corrected the values.

We also use an optional window to measure the Mgb index. We define the window between 5220 and 5234 Å. We have not found significant differences in the values of the Mgb index measured with the optional window with respect to the ones using the original band-passes in the sample of stars observed with the same instrumental configuration as NGC 4579 the same applied to the outer regions of the galaxy. However, our alternative window would have to be tested in a sample of normal galaxies. As it can be seen in Table 4, we obtain values very similar by using either our alternative window, or the technique proposed by GE96.

Table 4 shows the blue radial gradients of some indices in the central region where spectra show [NI] contamination. The different measured and corrected values are also displayed as follows: column 2 displays Mgb^0, the value of Mgb index measured with the original contaminated continuum band-pass, column 3, Mgb^1 the corrected value according to the measured Mgb^0 minus the contribution given by [NI] as in GE96 (formula 5), column 4 shows Mgb^2 the values of the Mgb index measured with our new spectral window. Column 5 gives the adopted value for the Mgb index, taken as the average between columns 3 and 4. Finally, column 6 gives the error associated taken as the maximum between the measurement errors and the differences between columns 3, 4 and the adopted value. Therefore this is the maximum error.

For the Mg molecular indices, Mg_1 and Mg_2, the strongest contaminating emission line is [OIII]4959 Å. Three optional windows were defined in Gorgas (1987) for elliptical galaxies in which [OIII] emission was present: one at the blue side of Mg_1 (5045 - 5071 Å); a second one at the red side of Mg_2 (5303 - 5367 Å), and a third one between both (5135 - 5157 Å). The average value of the first and second windows was used as the blue continuum for Mg_1 and Mg_2 indices. In our case (and may be in other similar spectra) the alternative continuum for Mg_1 is even more absorbed than the feature itself, and the information could be simply lost if these alternative windows were used. Therefore, to measure the magnesium molecular indices, we have removed the [OIII]λ 4959 Å line from the spectrum, and

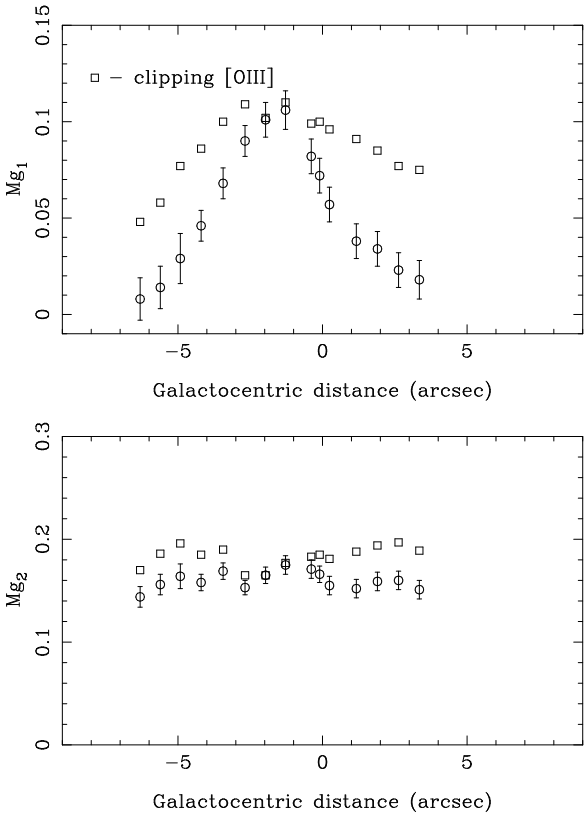

Fig. 3. Spatial gradients of Mg_1 (top) and Mg_2 (bottom) are displayed as a function of the galactocentric distance. Circles correspond to the values measured directly on the original spectra and open squares are those measured after removing the [OIII] λ 4959 Å

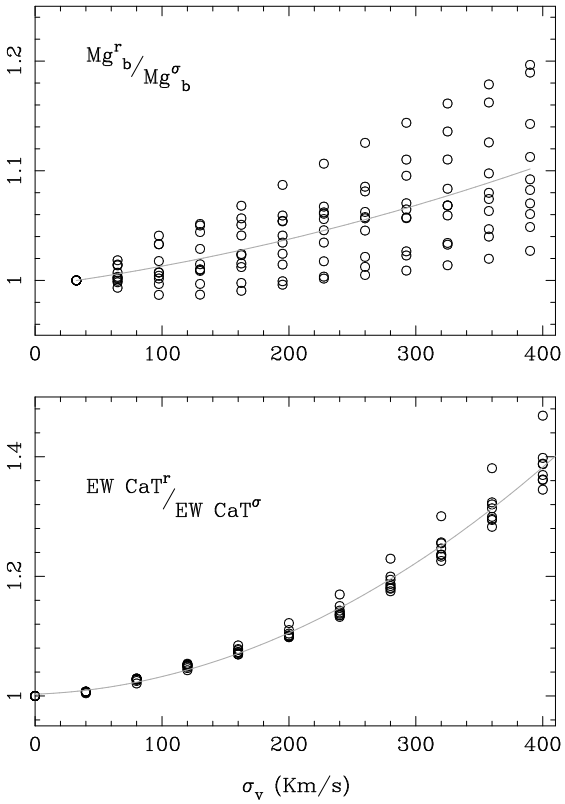

Fig. 4. Broadening correction curves for the Mgb and CaT indices. Y axis represents the ratio between the equivalent width measured in a stellar spectrum (at rest) and the same index measured in the broadened stellar spectrum. Different points correspond to different calibration stars observed during the night. A gaussian function was used to broaden the stellar spectrum.

then we have measured the indices with the standard continuum band-passes. To illustrate this effect, Fig. 3 shows the values of the molecular indices measured before (circles) and after (squares) removing the [OIII] 4959 Å line. The corrections are of the order of +0.02 mag. in Mg_2 and between +0.01 and +0.03 mag in the Mg_1 index.

Finally, in the case of the Mg_2 index, the contribution of the [NI] emission line has to be taken into account since it could contribute to the central window when the feature is measured, diluting the index. We have performed this correction after the previous one ([OIII] effect). Following Eq. (6) of GE96 we have calculated the corrective equivalent width of [NI]5200 Å inside the central value of the Mg_2 window in the way described above for the red window of the Mgb index. For the same galactocentric distances given in Table 4, the values of the corrections we have to add to the Mg_2 index are 0.010, 0.010, 0.010, 0.006, 0.007, 0.002 and 0.006 respectively.

When line indices are measured in galaxies, an extra-broadening of spectral absorption features appears due to the velocity dispersion of stars in the galaxy (see Terlevich et al. 1990). This afects the continuum producing smaller equivalent widths. To correct for this effect, a given spectral index is artificially broadened in the template stars by convolving their spectra with gaussians of different σ, and a broadening correction curve is built. Fig. 4 shows the broadening correction curves for Mgb in the blue and CaT in the near-IR. The best least-square fittings to the broadening correction curves (one per index) are given by the following equations:

$$Mgb^r = Mgb^\sigma(1 - 10^{-4} \times (4.4\sigma\ - 0.03\sigma^2))\ \text{Å} \quad (1)$$

$$Mg_1^r = Mg_1^\sigma(1 - 10^{-4} \times (1.79\sigma\ - 0.019\sigma^2))\ \text{mag} \quad (2)$$

$$Mg_2^r = Mg_2^\sigma(1 + 10^{-5} \times (7.52\sigma\ - 0.0015\sigma^2))\ \text{mag} \quad (3)$$

$$Fe_{52}^r = Fe_{52}^\sigma(1 - 10^{-5} \times (5.2\sigma\ - 0.4\sigma^2))\ \text{Å} \quad (4)$$

$$CaT^r = CaT^\sigma(1 + 10^{-5} \times (7.7\sigma\ + 0.2\sigma^2))\ \text{Å} \quad (5)$$

$$MgI^r = MgI^\sigma(1 - 10^{-5} \times (7.7\sigma\ - 0.9\sigma^2))\ \text{Å} \quad (6)$$

where r means the value at rest. For values of the Mgb index, measured with optional windows, the σ broadening correction expression is:

$$Mgb_{op}^r = Mgb_{op}^\sigma(1 + 10^{-4} \times (1.52\sigma\ - 0.003\sigma^2))\ \text{Å} \quad (7)$$

It is important to apply the corrections in this order: first the σ broadening correction, and then the optional window correction, if this was necessary (not in our case).

3.2. Kinematics

Stellar velocity dispersion measurements are needed to quantify the kinematics of the stellar population, and to obtain information about the central potential, responsible for the dynamics. The first method used to measure velocity dispersion was the Fourier Quotient Method (Sargent et al. 1977). Perhaps the method most commonly used nowadays is the cross-correlation technique (Tonry & Davies 1979) which requires the comparison with a stellar template. The velocity dispersion is derived from the width of the cross-correlation function after deconvolution from the instrumental profile. This procedure usually includes a filtering of high frequencies of the Fourier transform spectrum to avoid noise contamination and a low frequency filtering to eliminate the residual continuum.

At any rate, as pointed out by Dressler (1984) and Davies et al. (1987) the measured systemic velocity and σ are independent of the method used. Bottema (1988; 1989) used the whole profile of the cross- correlation function instead of the main peak only. The use of this method is possible only with high signal to noise spectra, obtained with long exposure times.

In this work, we use the cross-correlation method with slight differences with respect to the original one proposed by Tonry and Davies (1979). We consider a stellar spectrum as template which, after subtracting the continuum, is convolved with different gaussian functions (of different σ), simulating a large range in velocity dispersion. The gaussian-convolved spectra are cross-correlated with the unconvolved original stellar spectrum, and the width of the main peak of the cross-correlation function is measured. No frequency filtering is applied in this procedure. This method allows us to get a relation between this value (main peak's width) and σ of the input gaussian. Using then a polynomial fitting for values of σ higher than 70 Km/s we build the *correction curve* for each stellar template. We repeat this procedure for each of the stellar templates considered. To measure the velocity dispersion, σ, in a galactic spectrum, we convolve it (after continuum subtraction) with each stellar template, correcting the width of the main peak in the cross-correlation function according to the corresponding *correction curve*, obtaining σ. We considered σ as the average of the σ values found for each stellar spectrum used as template. This procedure allows a more precise measurement of σ. A very similar procedure has been used by Nelson & Whittle (1995). The main differences are: (a) they use an average stellar template instead of individual ones and (b) they filter high and low frequencies after the cross-correlation to avoid noise contamination and residual contributions to the continuum respectively.

The radial velocity, V_r, was measured using two methods:(a) through the shift between the spectrum and each of the templates (at rest), and (b) through the cross-correlation between the observed spectrum and an artificial template including δ functions at the positions of the 3 Mg lines (in the blue), and the 3 Ca lines (in the near-IR) The adopted V_r was the average of the two derived values.

The gas velocity dispersion has been measured by fitting a gaussian to the emission lines. Table 5 summarizes the results in row 1.

Table 5. Gas and stellar nuclear velocity dispersions for NGC 4579. Our data are compared with the ones in the literature (González-Delgado & Pérez 1996, GD96, Whitmore et al. 1985, W85; and Nelson & Whittle 1995, NW95). Note that σ_g (no [OIII]) refer to the value got by using all the emission lines except those corresponding to [OIII].

$\sigma(Km/s)$	Our work	W85	NW95	GD96
σ_g (no [OIII])	150 ± 20	—	—	—
σ_g ([OIII])	250 ± 17	—	278	238 ± 6
σ_s (CaT)	130 ± 13	—	—	185 ± 14
σ_s (MgI)	167 ± 17	185 ± 14	160 ± 11	—

The values for the stellar σ and V_r as function of the galactocentric radius are listed in columns 2 and 3 respectively in Tables 6 and 7.

4. Results: kinematics and index gradients in NGC 4579

4.1. Nuclear gas kinematics

The relation between the gas and stellar kinematics in the nucleus is interesting and the results are summarized in Table 5.

If the [OIII] lines are excluded, the mean velocity dispersion of the gas is 150 ± 20 Km/s, similar to that measured from the CaT (130 ± 13 Km/s) and Mg blue lines (167 ± 17 Km/s). The velocity dispersion from the [OIII] lines, 250 ± 17 Km/s, is however substantially larger than the stellar one, implying a different kinematics for the highly ionized gas and the stars in the nucleus of the galaxy. We have found indications of the existence of an extra component in [OIII], slightly broader and barely noticeable in Fig. 1, which might be associated with the remnants of emission bubbles (see Pogge 1989).

This behaviour of [OIII] has been observed also in another well studied LINER, NGC 1052 (Terlevich et al. 1990).

4.2. Stellar kinematical profiles

Figs. 5 and 6 show the rotation and the velocity dispersion curves for NGC 4579 as derived from the analysis of blue absorption lines (open squares) and near infrared ones (filled circles).

The rotation curve seems to be symmetric with respect to the nucleus. No significant differences are found between blue and near IR data although the radial velocity gradient seems to be slightly larger in the near IR (50 Km/s/arcsec) than in the blue (30 Km/s/arcsec). This can be explained as an obscuration effect. The near-IR observations reach deeper into the central region of the galaxy allowing the measurement of velocities closer to the nucleus. This effect has been observed in other galaxies, in particular in the starburst galaxies M82 (McKeith et al. 1993), NGC 2146 (Prada et al. 1994), and NGC 253 (Prada et al. 1996). In all of them, steeper velocity gradients were found for the lines in the near-IR than in the optical.

The stellar velocity dispersion distribution is rather flat both in the blue and near IR spectral regions. However, velocity dis-

Table 6. Blue gradients

r (arcsec)	σ (Km/s)	V_r (Km/s)	Mgb (Å)	Fe_{52} (Å)	Mg_1 (mag)	Mg_2 (mag)
–0.1	167 ± 17	1505 ± 67	3.23 ± 0.18	2.0 ± 0.5	0.100 ± 0.010	0.195 ± 0.010
+0.2	165 ± 17	1516 ± 67	3.24 ± 0.26	1.6 ± 0.5	0.096 ± 0.010	0.191 ± 0.010
–0.4	166 ± 17	1494 ± 70	3.29 ± 0.26	2.2 ± 0.5	0.099 ± 0.010	0.193 ± 0.009
+1.2	186 ± 19	1579 ± 78	2.99 ± 0.30	2.1 ± 0.5	0.091 ± 0.009	0.194 ± 0.009
–1.3	163 ± 16	1470 ± 64	3.00 ± 0.20	2.7 ± 0.6	0.110 ± 0.012	0.184 ± 0.011
+1.9	167 ± 17	1614 ± 70	3.23 ± 0.38	2.7 ± 0.3	0.085 ± 0.011	0.196 ± 0.011
–2.0	166 ± 17	1458 ± 63	2.51 ± 0.35	2.8 ± 0.6	0.102 ± 0.011	0.181 ± 0.011
+2.6	176 ± 18	1610 ± 38	3.21 ± 0.20	2.7 ± 0.2	0.077 ± 0.009	0.197 ± 0.009
–2.7	163 ± 16	1435 ± 64	3.02 ± 0.16	2.7 ± 0.4	0.109 ± 0.010	0.165 ± 0.009
+3.3	194 ± 19	1572 ± 37	3.12 ± 0.05	3.0 ± 0.2	0.075 ± 0.011	0.189 ± 0.011
–3.4	202 ± 20	1401 ± 53	2.90 ± 0.25	3.4 ± 0.5	0.100 ± 0.008	0.190 ± 0.008
+4.1	225 ± 45	1516 ± 45	—	—	—	—
–4.2	154 ± 23	1392 ± 60	2.67 ± 0.36	2.7 ± 0.3	0.086 ± 0.008	0.185 ± 0.008
+4.8	221 ± 40	1518 ± 26	—	—	—	—
–4.9	168 ± 37	1428 ± 25	2.37 ± 0.52	3.1 ± 0.5	0.077 ± 0.013	0.196 ± 0.013
+5.5	171 ± 17	1553 ± 27	—	—	—	—
–5.6	157 ± 33	1444 ± 24	—	—	—	—
+6.2	199 ± 37	1518 ± 31	—	—	—	—
–6.3	194 ± 20	1535 ± 53	—	—	—	—

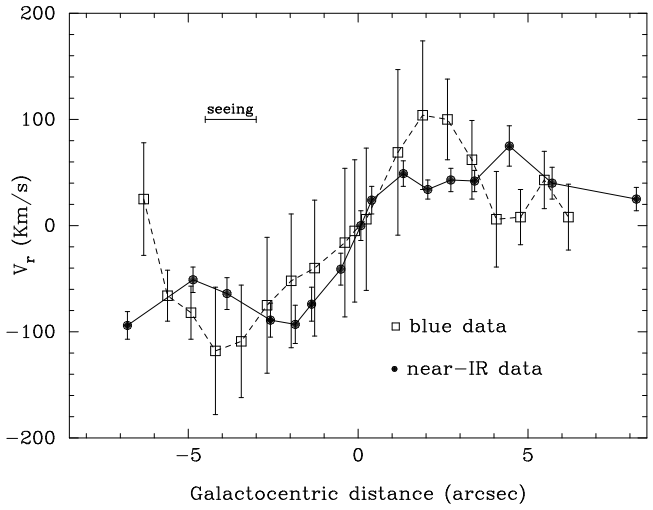

Fig. 5. Rotation curve for NGC 4579 (1"= 97 pc; assuming a distance of 20 Mpc and H_0 = 75 $Kms^{-1}Mpc^{-1}$)

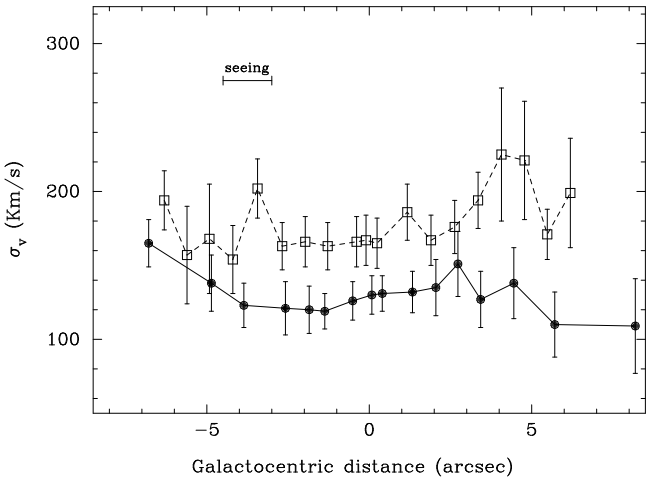

Fig. 6. Velocity dispersion profile derived from the Mgb lines in the blue and the CaT lines in the near-IR

persions derived from the blue lines are systematically larger than those derived from the near IR ones. We believe that this difference (30-40 Km/s) cannot be due solely to observational errors. Considering that GD96 measured a velocity dispersion much larger than ours, we conclude that more observations are needed to check this effect.

4.3. Gradients of spectral indices

We have measured the Mgb, Mg_1, Mg_2 and Fe_{52} indices in the blue range, and CaT and MgI, in the near-IR, studying their spatial variations in the central 1.5 Kpc. Fig. 7 illustrates the spatial spectral gradient. Blue (left panels) and near-IR (right panels) spectra at two extreme positions from the nucleus are shown. Fig. 8 shows the spatial variation of the six measured spectral indices, whose values are given in Tables 6 and 7.

No dilution of Mgb index is observed in the nucleus of the galaxy. For values of the galactocentric distance out of the 2.5 central arcsec, no emission is found and therefore the standard windows have been used. For the central region we have adopted the values listed in Table 6 and discussed in Sect. 3.1.

The blue Mg_1 and the IR MgI indices show a radial gradient, stronger for the later one, with the index increasing to the centre and reaching the maximum value at around -1.4" from

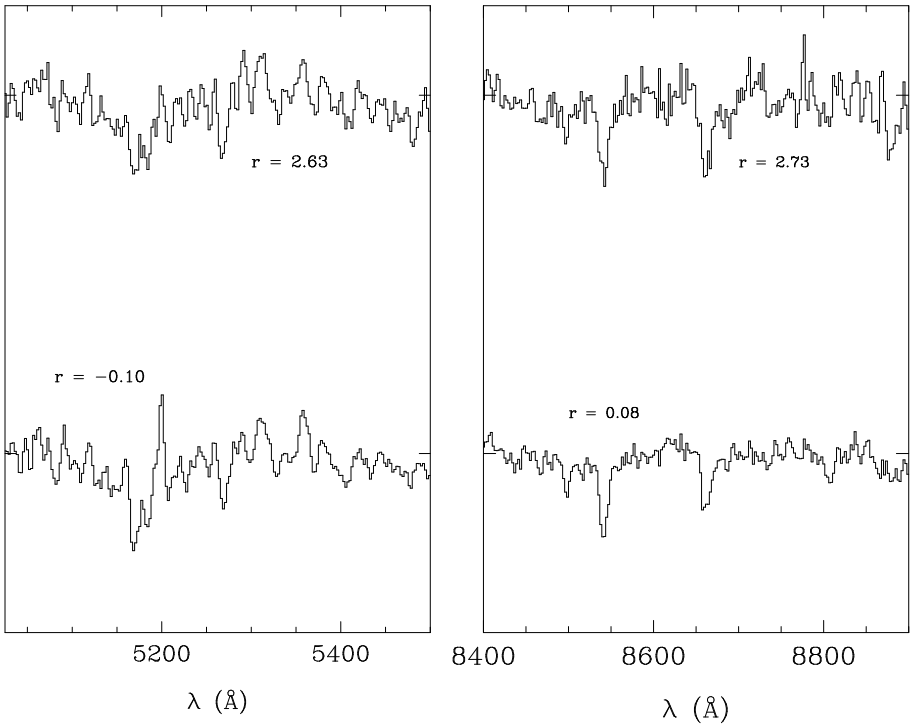

Fig. 7. Representative spectra at two different galactocentric distances (r in arcsec). Left panels correspond to blue spectra and spectra at the right are the corresponding ones in the near-IR. The spectra have been normalized, dividing them by the continuum

Table 7. Near-IR gradients

r (arcsec)	σ (Km/s)	V_r (Km/s)	CaT (Å)	MgI (Å)
+0.1	130 ± 13	1586 ± 14	6.5 ± 0.3	0.97 ± 0.04
+0.4	131 ± 12	1610 ± 13	6.5 ± 0.5	0.71 ± 0.06
–0.5	126 ± 13	1545 ± 15	6.9 ± 0.2	1.16 ± 0.05
+1.3	132 ± 14	1635 ± 12	5.9 ± 0.5	0.58 ± 0.09
–1.4	119 ± 12	1512 ± 16	6.5 ± 0.2	1.10 ± 0.04
+2.1	135 ± 19	1620 ± 9	6.3 ± 0.5	—
–1.8	120 ± 16	1493 ± 18	6.7 ± 0.1	0.79 ± 0.05
+2.7	151 ± 22	1629 ± 11	6.9 ± 0.5	—
–2.6	121 ± 18	1497 ± 16	6.5 ± 0.3	0.45 ± 0.05
+3.4	127 ± 19	1628 ± 10	6.5 ± 0.6	—
–3.9	123 ± 15	1522 ± 15	6.8 ± 0.3	—
+4.4	138 ± 24	1661 ± 19	6.0 ± 0.4	—
–4.9	138 ± 19	1535 ± 12	6.9 ± 0.5	—
+5.7	110 ± 22	1626 ± 15	6.9 ± 0.7	—
–6.8	165 ± 16	1492 ± 13	7.0 ± 0.5	—
+8.2	109 ± 32	1611 ± 11	7.4 ± 0.5	—

the nucleus. This could be the result of an increasing metallicity towards the centre of the galaxy.

This behaviour is not shared by the Mg_2 index for which a constant value of 0.195 ± 0.010 mag is found in the central 10 arcsec of the galaxy. [NI] emission at 5200 Å contaminates the measured index in the nuclear spectrum since the band-pass for the Mg_2 feature extends to 5197.25 Å (see also Sect. 3.1). However, no significant gradient is found either when the central two increments (the two showing emission lines) are excluded.

The measured CaT is also rather constant through the central 10 arcsec of the galaxy with a mean value of 6.5 ± 0.5 Å (consistent with the result of an almost flat gradient found by González-Delgado & Pérez 1996, with an average value of 6.4 Å). The fact that neither dilution nor enhacement of the CaT lines is observed indicates that they probably correspond to the bulge underlying population.

Finally, the Fe_{52} index is found to be substantially diluted in the centre with respect to that measured in normal bulges. Such a dilution cannot be attributed to the ionizing continuum responsible for the activity of the AGN since in that case the Mgb index should also appear diluted. Weak [FeII] emission concentrated in the galaxy nucleus might be responsible for the observed weakening of the absorption lines. In fact, UV spectra of NGC 4579 obtained with IUE (Reichert et al. 1992) also show blended [FeII] emission. This has been confirmed in the FOS/HST spectrum of the nucleus of this galaxy by Barth et al. (1996). Apart from this dilution, the average value of the index out of the nucleus is 2.9 ± 0.5 Å and no spatial gradient is found. For the stellar population analysis in the central region, we have averaged the values of the indices between +0.5" and -1.5" except in the case of Fe_{52}. The value we have adopted for this index is 2.7 Å since this is the only non-contaminated observation which is still in this region (at r = -1.3") according to the rotation curve (see Fig. 5), but it has to be considered only as an estimation.

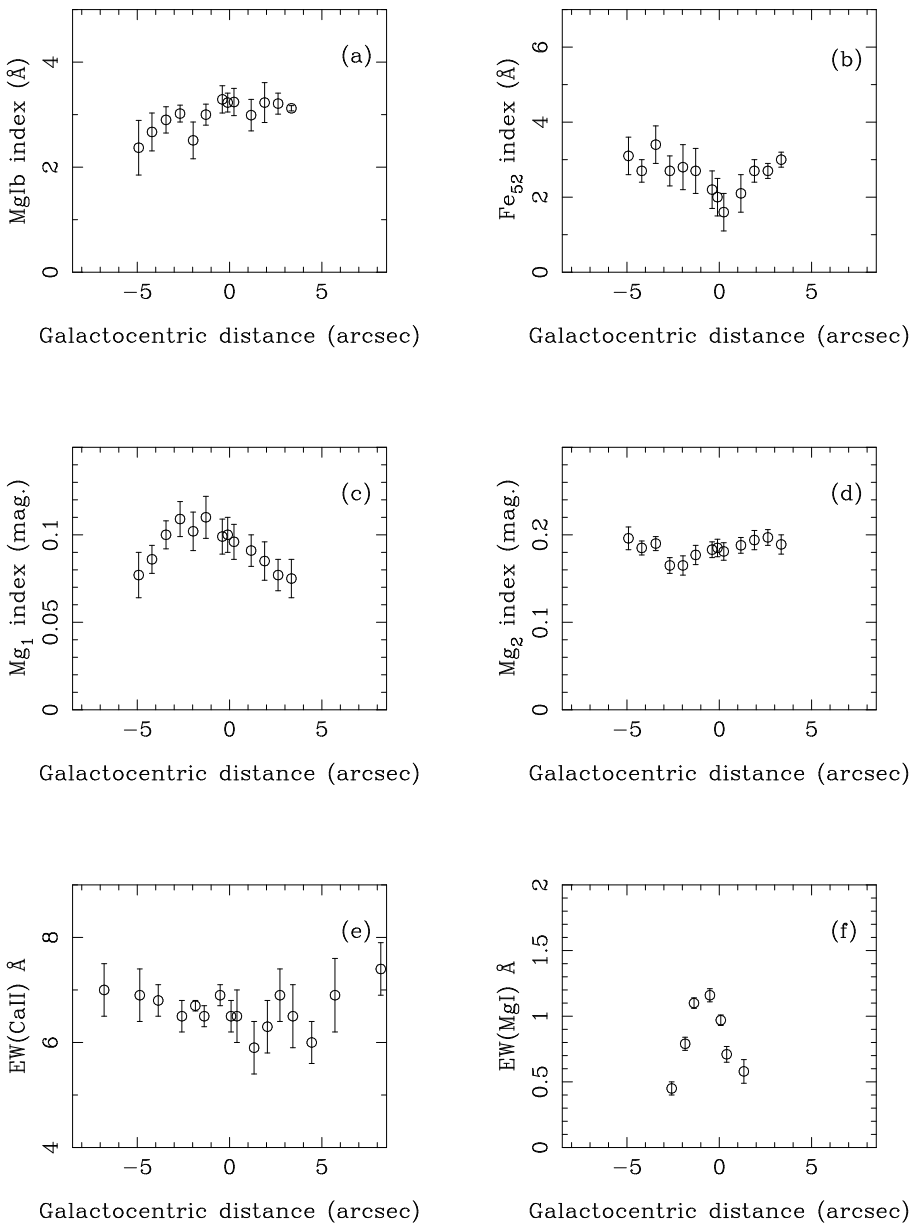

Fig. 8a–f. Spectral index gradients: Mgb, Fe_{52}, Mg_1 and Mg_2 blue indices and CaT and MgI 8807 in the near-IR are shown as a function of the galactocentric distance in panels **a**, **b**, **c**, **d**, **e** and **f** respectively

5. Discussion: constraints for the age and metallicity of the parent galaxy

To interpret our results we have used the most recent models available to compute the stellar indices as a function of the age and the metallicity for Single Stellar Populations (SSP).

Worthey (1994) presented evolutionary synthesis models for SSP as a function of the metallicity, based on the revised Yale isochrones (Green et al. 1987), the atmosphere models by Kurucz (1992) and the stellar atlases of Bessell et al. (1989, 1991) and Gunn & Stryker (1983). He synthesized 21 absorption stellar indices using the fitting functions calculated by Worthey et al. (1994) in which each index is a function of the stellar effective temperature, surface gravity and metallicity.

According to Worthey's (1994) work, the model which best reproduces our results for the nuclear stellar population corresponds to a SSP with an age around 3 Gyr and solar metallicity. Alternatively, if a higher metallicity model (1.7 $Z_\odot$) is chosen, the population should be even younger, 1.5-2 Gyr. A model of 0.5 $Z_\odot$ and around 12 Gyr would also fit the observed values within the errors. Models for ages older than 12 Gyr would give too large values of both, Mg_2 and Mg_b indices. Table 8 summarizes Worthey's predictions for these models, and our results for NGC 4579.

Casuso et al. (1996) have computed the Mg_2 index as a function of age and metallicity. They also use the fitting functions by Worthey et al. (1994) to calculate the index for each particular star in the HR diagram. The improvement with respect to previous models (Peletier 1989; Worthey 1994) resides in the use of the Padova isochrones (Bertelli et al. 1994), which include

Table 8. Comparison between the observations of the nuclear blue stellar indices for NGC 4579 and SSP models computed by Worthey (1994)

Z $Z_\odot$	Age Gyr	Mg_1 mag	Mg_2 mag	Mgb Å	Fe_{52} Å
1	1.5	0.06	0.16	2.4	2.3
1	2	0.07	0.19	2.8	2.6
1	3	0.08	0.21	3.1	2.7
1	5	0.08	0.22	3.3	2.8
1.7	1.5	0.08	0.20	2.8	2.7
1.7	2	0.09	0.23	3.3	2.9
0.3	12	0.06	0.17	2.7	2.3
1	12	0.11	0.26	3.9	3.1
0.6	17	0.09	0.23	3.6	2.8
1	17	0.12	0.28	4.1	3.2
1	17	0.12	0.28	4.1	3.2
Obs		0.10	0.195	3.2	2.7
		$\pm$ 0.01	$\pm$ 0.01	$\pm$ 0.3	$\pm$ 0.5

better opacity Tables and a detailed treatment of the advanced stages of stellar evolution, in particular the AGB phase.

According to these models, a value of the Mg_2 index as low as 0.195 mag can only be found in two very different populations: either a relatively low metallicity (around 0.3 - 0.4 $Z_\odot$) old bulge (12 Gyr), or a younger (1 - 2 Gyr) metal rich (1 - 2 $Z_\odot$) population. The first possibility would reproduce the indices, although the values of Mg_1 in the blue and the atomic MgI in the near-IR seem to point to a higher metallicity scenario. The second possibility is in agreement with Worthey's results presented above, showing an age between 1.5 and 3 Gyr and a metallicity between $Z_\odot$ and 1.7 $Z_\odot$. In fact, the low value of Mg_2 index (0.195 mag) found in the whole central region of NGC 4579 places this galaxy out of the correlation of Mg_2 versus σ found for elliptical galaxies (0.28 mag according to the relation given in Bender et al. 1993 and references therein), and S0 galaxies (Fisher et al. 1996 and references therein). However, NGC 4579 with a bulge magnitud of -19.2 (Simien & de Vaucouleur 1986) and σ(Mg) of 167 $\pm$ 17 Km/s follows the M_B vs σ relation found for elliptical and normal spirals (see Terlevich et al. 1990). These two facts taken together imply that the value of the Mg_2 index for this galaxy is abnormally low for its bulge luminosity and points to a difference in the dominant stellar population in the nucleus of NGC 4579. This fact supports the idea that low values of the Mg_2 are found in galaxies in which there are indications of star-forming processes occurred after the galaxy formation. In fact, lower values of this index have been found in elliptical galaxies with nuclear emission (González 1993; Fisher et al. 1996) and galaxies with strong cooling flows (Cardiel et al. 1996). Moreover, data from Fisher et al. (1996) reveal that the flattest Mg_2 gradients, also showing the lowest values for the index, are found in galaxies with nuclear emission.

Recently, Vazdekis et al. (1996), have computed evolutionary synthesis models for early-type galaxies, with metallicities 0.4 $Z_\odot$, $Z_\odot$, and 2.5 $Z_\odot$ and ages 1, 4, 8, 12 and 17 Gyr. The models are also based on Padova's tracks and they are an extension of those presented in Casuso et al. (1996). They have considered different hypotheses about the IMF, the chemical evolution and the star formation history, producing a set of models which includes colours and line indices, in particular all the indices studied here for NGC 4579. For the blue ones they enter in their code the fitting functions given by Worthey et al. (1994).

Regarding the near-IR indices, the CaT and MgI can also be used to constrain the properties of stellar populations with the help of evolutionary synthesis models.

In individual stars, the behaviour of the CaT as a function of stellar effective temperature, surface gravity and metallicity has been studied in detailed both empirically (Jones et al. 1984; Díaz et al. 1989, Zhou 1991; Mallik 1994) and theoretically (Jørgensen et al. 1992). The surface gravity is the parameter governing the strength of the CaT in high metallicity systems (Z > 0.5 $Z_\odot$), with the CaT increasing with decreasing gravity. For metallicities as low as 0.3 $Z_\odot$, the effects of surface gravity and effective temperature become competitive. Finally, the effect of the metal abundance is found to be important only in metal-poor giants and supergiants with a lower metallicity producing a lower EW(CaT).

With respect to the behaviour of the IR MgI 8807 Å line in stars, it has been studied by Díaz et al. (1989) who found its equivalent width to depend on both effective temperature and metallicity, with the EW(MgI) increasing with increasing metallicity and decreasing effective temperature.

Vazdekis et al. (1996) have published the synthetic values for the CaT and MgI based solely on Díaz et al. (1989) calibration, which does not include the coolest late-type stars and only few high metallicity stars. These problems lead to fitting functions for CaT and MgI which can give overestimated values for CaT in very old population (in which cool giants are dominating the near-IR spectrum) and underestimated values of MgI for metal-rich populations.

In fact, if Vazdekis' models are used, the predicted value of the CaT is (8.2 $\pm$ 0.5) Å, independently on the age at solar metallicity, for all their published SSP (1-17 Gyr) with Z $\geq$ $Z_\odot$ which is not in agreement with the observations of CaT in elliptical galaxies (Terlevich et al. 1990; Delisle & Hardy 1992, Gorgas et al. 1996). With respect to the MgI index, the inclusion of only few high metallicity stars, and the strong dependence on metallicity of this index, could lead to an underestimation of the index for metal-rich (higher than solar) populations.

García Vargas et al. (1997) have computed equivalent widths of the CaT for SSP of different metallicities (2.5 $Z_\odot$, $Z_\odot$, 0.4 $Z_\odot$ and 0.2 $Z_\odot$) synthesized using a standard Salpeter-type initial mass function (IMF) and ranging in age from 1 Myr to 15 Gyr. The models are based on Padova stellar tracks (Bressan et al. 1993, Fagotto et al. 1994a, b) and the CaT equivalent widths have been calculated with both, theoretical models (Jørgensen et al. 1992) and empirical data (Díaz et al. 1989; Zhou 1991). These models include a calibration for the late-type cool stars and use a more appropriate abundance calibra-

Table 9. Comparison between the nuclear observations and models of stellar indices for NGC 4579. All the indices are taken from Vazdekis et al. (1996) except the CaT which has been taken from García-Vargas et al. (1997).

Z $Z_\odot$	Age Gyr	Mg_1 mag	Mg_2 mag	Mgb Å	Fe_{52} Å	CaT Å	MgI Å
1	1	0.034	0.123	2.1	2.0	5.8	0.64
1	3	0.070	0.186	2.9	2.5	7.1	0.74
1	4	0.089	0.218	3.4	2.8	7.2	0.79
2	2	0.080	0.191	3.0	2.7	6.9	0.80
2.5	1	0.064	0.172	2.6	2.6	7.2	0.84
1	10	0.114	0.263	3.9	3.1	7.3	0.84
0.4	12	0.081	0.202	3.2	2.6	5.9	0.73
0.4	17	0.092	0.216	3.3	2.7	5.9	0.77
Obs		0.10	0.195	3.2	2.7	6.5	0.98
		$\pm$ 0.01	$\pm$ 0.01	$\pm$ 0.3	$\pm$ 0.5	$\pm$ 0.5	$\pm$ 0.1

tion based on the theoretical models by Jørgensen et al. (1992), but see the discussion in García-Vargas et al. (1997).

We have used the models described above to constrain the age of the dominant stellar population. For the predictions of CaT we have taken the models by García-Vargas et al. (1997). For MgI, since the only available models are those of Vazdekis et al. (1996) we have used them but we have to keep in mind that they could be only lower limits to the real value (especially in their models at $Z \geq Z_\odot$).

Table 9 presents a comparison between the observations and models of the studied stellar indices in NGC 4579. All the computed indices have been taken from Vazdekis et al. (1996) except the CaT which has been taken from García-Vargas et al. (1997). Both set of models are computed with the same evolutionary scheme (Padova's isochones of SSP) and for a unimodal standard (Salpeter) IMF. Some models interpolated between the original ones (3 Gyr and 10 Gyr at $Z_\odot$ and 2 Gyr at 2 $Z_\odot$) are also given for comparison.

The blue indices, specially the strong constraint given by the low Mg_2 index, again point to the same conclusion reached from Worthey's models. The solution is not single-valued and the observations are consistent with an old bulge (see model at 0.4 $Z_\odot$ and 12 Gyr) or alternatively with a younger population (see model at 2 $Z_\odot$ and 2 Gyr).

From the near-IR indices, the models indicate that the observed EW(CaT) in NGC 4579 can be originated in a population with a metallicity about solar and an age between 1 and 2 Gyr. Such a population produces an EW(CaT) of 6.5 $\pm$ 0.5 Å which is also the observed value. However, the value of CaT is also quite consistent with an old 0.4 $Z_\odot$ population (5.9 $\pm$ 0.5 Å).

The IR MgI line gradient found in the central region of NGC 4579 could therefore be interpreted as a gradient in metallicity since more metal rich stars would in general also be cooler, both effects combining to produce IR MgI line.

All the evidence seem to indicate that the physical parameters of the dominant central population in NGC 4579 could correspond to a high metallicity system (around $Z_\odot$) substantially younger than a typical old bulge population. Current population synthesis models of SSP place its age between 1 and 3 Gyr.

Previous works have pointed to an old population, suggested on the basis of the optical spectral energy distribution. Stauffer (1982) showed a low dispersion spectrum of the nucleus of NGC 4579, finding that a template population like that of the E galaxy NGC 3379 would be suitable. In fact, NGC 4579 was classified by Bica (1988) in the spectral group S3, which is red strong lined like those of E3 and E2 (like NGC3379 and other typical E and S0), although inspection of Fig. 12 (S3) and 13 (S4) from Bica (1988) and the observed spectra by González-Delgado & Pérez (1996, see Fig. 8a), indicates that this galaxy can be classified as S4, for which an intermediate population (1-5 Gyr) is expected contributing less than 20% to the light in the blue.

To test again both possibilities, we have compared models of SSP with the observed spectrum of NGC4579. Bica & Alloin (1987a) present data for NGC4579 up to 7520 Å, but the galaxy is not included in their near-IR sample (Bica & Alloin 1987b). To have a wider wavelength range we have used the optical spectrum of M58 kindly provided by E. Pérez (see González-Delgado & Pérez 1996). For the models, we have taken those SSP published by Padova's group and kindly provided by A. Bressan. The specifications of their models are described in Tantalo et al. (1996) and Bressan et al. (1996). We have reddened the SSPs with a value of E(B-V)=0.15 mag (Barth et al. gives a value between a minimum of 0.10 and a maximum of 0.19 mag for the nucleus of NGC4579). The spectrum provided by González-Delgado & Pérez and the two SSPs which best fit the SED, provided by A. Bressan are displayed in Fig. 9.

The observed values for the continuum flux ratios at the specified wavelengths in Å 4020/5870, 4570/5870, 5340/5870, 6630/5870, 6990/5870, 7790/5870, 8310/5870, 8890/5870, 9430/5870, 9610/5870 and 9790/5870 are: 0.51, 0.79, 0.92, 1.02, 0.99, 0.95, 0.91, 0.99, 0.96, 1.01 and 1.1 respectively. The synthetic values for a SSP of 2 $Z_\odot$ and 2 Gyr are 0.51, 0.84, 0.90, 0.97, 0.96, 0.92, 0.89, 0.94, 0.95, 0.97 and 0.93. The comparison shows that the model and the observations are in agreement. If we take a SSP of 12 Gyr and Z=0.008, the predicted values for the same ratios are: 0.46, 0.79, 0.90, 1.00, 0.99, 0.96, 0.93, 0.95, 0.92, 0.91 and 0.87, also consistent. Both populations, a youngest metal-rich or an old metal-poor can fit the SED.

Finally, if models with a SFR and chemical evolution are taken (Vazdekis et al. 1996) the observations are consistent with a stellar population of (7 $\pm$ 3) Gyr, a SFR of (10 $\pm$ 5) $\times$ 10^{-4} $M_\odot yr^{-1}$, and an average solar metallicity.

6. Conclusions

We have studied the kinematics and stellar population in the central regions of the LINER galaxy NGC 4579 by using long slit spectroscopic observations in the blue and near-IR.

From the kinematical study, we find a marginally steeper radial gradient in the near-IR (CaT) velocity curve which we

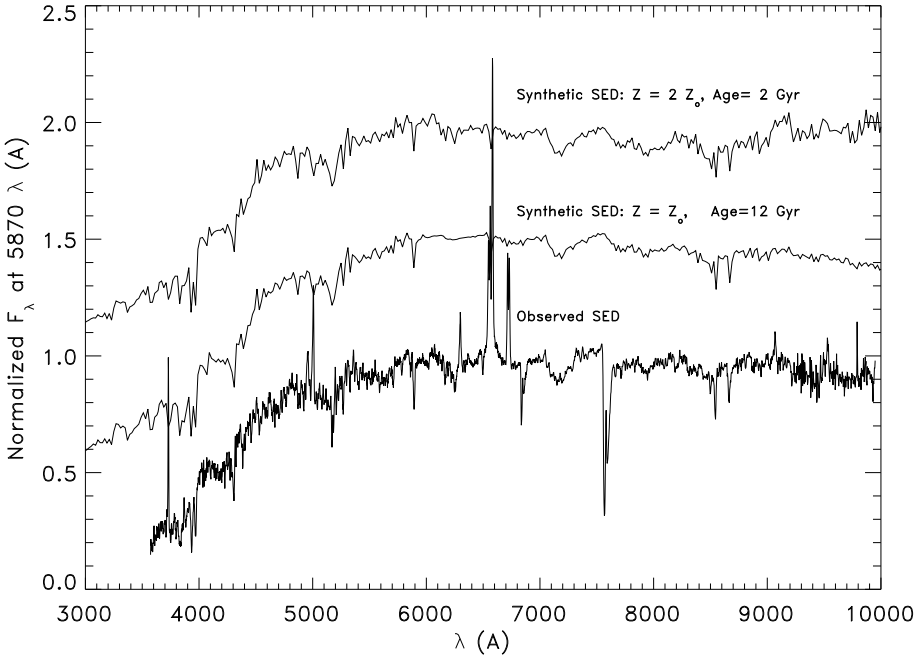

Fig. 9. Spectral Energy Distribution of NGC4579. The observed spectrum is from González-Delgado & Pérez 1996. The SSPs are taken from the Padova's grid. The SSP at $Z_\odot$ and 12 Gyr have been taken directly from the grid and the SSP at 2 $Z_\odot$ has been computed by interpolating in metallicity between the original SSPs at 2 Gyr and metallicities $Z_\odot$ and 2.5 $Z_\odot$.

attribute to the smaller line-of-sight optical depth and hence a deeper penetration into the dusty nucleus. We also find a discrepancy between the velocity dispersions measured form the MgI blue lines and CaT lines with the latter ones producing smaller values. This discrepancy should be investigated to find if this is a true effect. In any case, the velocity dispersion is rather flat with no central cusp.

Regarding the stellar populations, we find some indications of a positive metallicity gradient towards the centre of the galaxy. We do not find any real dilution of the stellar indices due to the presence of a blue nuclear continuum. Fe_{52} is the only index which shows a clear dilution, what we attribute to contamination by [FeII] emission.

An old (12-17 Gyr) population, typical of normal elliptical and S0 galaxies would be only marginally compatible with the Mg_2 index, although able to reproduce the rest of the observational constraints. Alternatively, and according to various recent population synthesis models, we propose that the parent galaxy of the LINER nucleus could have a central underlying population of about solar metallicity and an age of about (2.5 ± 1) Gyr. If an older age with this high metallicity was assumed, an active star formation during the life of the galaxy was required to reproduce the observations. Unfortunately, from our data and within the observational errors, we cannot provide a definitive solution for the dominant bulge population in this LINER. Both models (young metal-rich and older metal-poor) are possible. Observations with higher spatial and spectral resolution are needed in this galaxy and in other LINERs to find a conclusive solution.

Finally, we have showed how the near-IR spectrum, through the metallicity-dependent indices CaT and MgI, can help to constrain the physical properties of the stellar populations, especially in the objects whose nuclear emission is contaminating the blue spectrum. The developement of models for MgI in the near-IR is needed.

Acknowledgements. J. Palacios thanks the support by the UAM research fellowship. We thank E. Pérez and A. Bressan for kindly providing us the whole optical spectrum of NGC4579 and the SSP's models respectively, and Rosa González, Charlie Nelson and Javier Gorgas for fruitful discussions. We thank the useful comments and suggestions from the anonymous referee which have contributed significatively to the improvement of the paper. This work has been partially supported by a British Council grant for collaborative research.

References

Barth A.J., Reichert G.A., Filippenko A.V., Ho, L.C., Shields J. C., Mushotzky R.F., & Puchnarewicz E.M., 1996, AJ, 112, 1829
Bender R., Burstein D. & Faber S.M., 1993, ApJ, 411, 153
Bertelli G., Bressan A., Chiosi C., Fagotto F. & Nasi 1994, A&AS, 106, 275
Bessell M.S., Brett J.M., Scholz M. & Wood P.R., 1989, A&AS, 77, 1
Bessell M.S., Brett J.M., Scholz M. & Wood P.R., 1991, A&AS, 89, 335
Bica E., 1988, A&A, 195, 76
Bica E. & Alloin D., 1987a, A&AS, 70, 281
Bica E. & Alloin D., 1987b, A&A, 186, 49
Bottema R., 1988, A&A, 197, 105
Bottema R., 1989, A&A, 221, 236
Bressan A., Fagotto F., Bertelli G., & Chiosi C., 1993, A&AS, 100, 647
Bressan A., Chiosi C. & Tantalo R., 1996, A&A, 311, 425
Cardiel N., Gorgas J. & Aragón Salamanca A., 1996, MNRAS, 277, 502
Casuso E., Vazdekis A., Peletier R.F. & Beckman J.E., 1996, ApJ, 458, 533
Davies R.L., Burstein D., Dressler A., Faber S.M., Lynden-Bell D., Terlevich R. & Wegner G., 1987, ApJS, 64, 581
Delisle S. & Hardy E., 1992, AJ, 103, 711
de Vaucoleurs G., de Vaucoleurs A., Corwin H.G., Buta R.J., Paturel G. & Fouqué P., 1991, *Third Reference Catalogue of Bright Galaxies*, Springer-Verlag.

Díaz A.I., Terlevich E. & Terlevich R., 1989, MNRAS, 239, 325
Dressler A., 1984, ApJ, 281, 512
Fagotto F., Bressan A., Bertelli G., Chiosi C., 1994a, A&AS, 104, 365
Fagotto F., Bressan A., Bertelli G., Chiosi C., 1994b, A&AS, 105, 29
Filippenko A.V. & Sargent W.L.W., 1985, ApJS, 57, 503
Fisher D., Franx M. & Illingworth G., 1996, ApJ, 459, 110
García-Vargas M.L., Mollá M. & Bressan A., 1997, submitted
González J.J., 1993, PhD Thesis. Univ. California.
González-Delgado R.M. & Pérez E., 1996, MNRAS, 281, 1105
Gorgas J., 1987, PhD Thesis. Univ. Complutense, Madrid
Gorgas J., Faber S.M., Burstein D., González J., Courteau S. & Prosser C., 1993, ApJS, 86, 153
Gorgas J., García-Vargas M.L. & Cardiel, 1996, in preparation
Goudfrooij P. & Emsellem E., 1996, A&A, 306, L45
Green E.M., Demarque P. & King C.R., 1987, *The Revised Yale Isochrones and Luminosity Functions* (New Haven: Yale University Observatory)
Gunn J.E. & Stryker L.L., 1983, ApJS, 52, 121
Halpern J.P. & Steiner J.E., 1983, ApJ, 269, 37
Hummel E., Van der Hulst J.M. & Dickey J.M., 1984, A&A, 134, 207
Hummel E., Van der Hulst J.M., Keel W.C. & Kennicutt R.C.Jr, 1987, A&AS, 70, 517
Hummel E., Van der Hulst J.M., Kennicutt R.C.Jr & Keel W.C., 1990, A&A, 236, 333
Jones J.E., Alloin D.M. & Jones B.J.T., 1984, ApJ, 283, 457
Jørgensen U.G., Carlsson M. & Johnson H.R., 1992, A&A, 254, 258
Keel W.C., 1983, ApJ, 269, 466
King D.L., 1985, La Palma Technical Note No. 15
Kinney A.L., Bohlin R.C., Calzetti D., Panagia N. & Wyse R.F.G, 1993, ApJS, 86, 5
Kurucz R., 1992, *Precision Photometry: Astrophysics of the Galaxy*, ed. P.G. Davis Phillip, A.R. Upgren & K.A. Janes, L. Davis press, Schenectady
Mallik S.V., 1994, A&AS, 103, 279
Maoz D., Filippenko A.V., Ho L.C., Rix H.W., Bohcall J.N., Schneider D.P. & Macchetto F.D., 1995, ApJ, 440, 91
Mc Keith C.D., Castles J., Greve A., Downes D., 1993, A&A, 272, 98
Nelson C.H. & Whittle M., 1995, ApJS, 99, 67
Oke J.B. & Gunn J.E., 1983, ApJ, 266, 713
Peletier R.F., 1989, PhD Thesis, Univ. Groningen
Pogge R.W., 1989, ApJS, 71, 433
Prada F., Beckman J.E., Castles J., McKeith C.D. & Greve A., 1994, ApJ, 423, L35.
Prada F., Manchado A., Canzian B., Peletier R.F., McKeith C.D. & Beckman J.E., 1996, ApJ, 458, 537.
Reichert G., Branduardi-Raymont G., Filippenko A.V., Mason K.O., Puchnarewicz E.M. & Wu C., 1992, ApJ, 387, 536
Reichert G., Puchnarewicz E.M., Filippenko A.V., Mason K.O. & Branduardi-Raymont G., 1993, in *The Nearest Active Galaxies*, eds. J. Beckman, L. Colina & H. Netzer, CSIC, p. 85
Sargent W.L.W, Schester P.L., Bocksenberg A. & Shortridge K, 1977, ApJ, 212, 326
Simien F. & de Vaucouleurs G., 1986, ApJ, 302, 564
Stauffer J.R., 1982, ApJ, 262, 66
Tantalo R., Chiosi C., Bressan A. & Fagotto F., 1996, A&A, 311, 361
Terlevich E., Díaz A.I. & Terlevich R., 1990, MNRAS, 242, 271
Tonry J.L. & Davies M., 1979, AJ, 84, 1511
Vazdekis A., Casuso E., Peletier R.F. & Beckman J.E., 1996, ApJS, 106, 307
Véron-Cetty M.P. & Véron P., 1993, *A Catalogue of Quasars and Active Nuclei*
Whitmore B.C., McElroy D.B. & Tonry J.L., 1985, ApJS, 59, 1
Whorthey G., 1994, ApJS, 95, 107
Whorthey G., Faber S.M., González J.J. & Burstein D., 1994, ApJS, 94, 687
Zhou X., 1991, A&A, 248, 367

This article was processed by the author using Springer-Verlag LaTeX A&A style file *L-AA* version 3.